Atmos. Chem. Phys. Discuss., 8, 20399–20425, 2008
www.atmos-chem-phys-discuss.net/8/20399/2008/

Atmospheric Chemistry and Physics Discussions

This discussion paper is/has been under review for the journal *Atmospheric Chemistry and Physics (ACP)*. Please refer to the corresponding final paper in *ACP* if available.

Effects of model resolution on entrainment (inversion heights), cloud-radiation interactions, and cloud radiative forcing

H. Guo[1], Y. Liu[1], P. H. Daum[1], X. Zeng[2,3], X. Li[2,3], and W.-K. Tao[3]

[1]Atmospheric Science Division, Brookhaven National Laboratory, Upton, NY, USA
[2]Goddard Earth Sciences and Technology Center, University of Maryland at Baltimore County, Baltimore, Maryland, USA
[3]Laboratory for Atmospheres, NASA Goddard Space Flight Center, Greenbelt, Maryland, USA

Received: 24 June 2008 – Accepted: 7 October 2008 – Published: 8 December 2008

Correspondence to: H. Guo (hguo@bnl.gov)

Published by Copernicus Publications on behalf of the European Geosciences Union.

Abstract

We undertook three-dimensional numerical studies of a marine stratus deck under a strong inversion using an interactive shortwave- and longwave-radiation module. A suite of sensitivity tests were conducted to address the effects of model resolution on entrainment (inversion heights), cloud-radiation interactions, and cloud radiative-forcings by varying model horizontal resolution only, varying vertical resolution only, and varying horizontal- and vertical-resolution simultaneously but with a fixed aspect ratio of 2.5.

Our results showed that entrainment (inversion height) is more sensitive to vertical- than to horizontal-resolution. A vertical resolution finer than 40 m can simulate spatial- and temporal-variations in the inversion height well. The inversion height decreases with increasing vertical resolution, but tends to increase with increasing horizontal resolution. Cloud liquid water path doubles after refining both the vertical- and horizontal-resolution by a factor of four. This doubling is associated with a positive feedback between cloud water and cloud top radiative cooling, which amplifies small differences initiated by changes in the model resolution. The magnitude of the cloud radiative-forcing tends to increase with increasing model resolution, mainly attributable to the increase in the cloud liquid water path. Shortwave radiative forcing is dominant, and more sensitive to model resolution than the longwave counterpart.

1 Introduction

Clouds largely determine the albedo of the Earth-atmosphere system. Cloud radiative forcing is critical for the global radiative and/or energy budget, and is thereby of profound importance for projecting future climate changes. Clouds are highly inhomogeneous over multiple scales both spatially and temporally. This multi-scale inhomogeneity can exert a noticeable effect on the radiative flux (Cahalan, 1994; Chen et al., 2000), while inhomogeneous radiative cooling/heating, in turn, substantially impacts

cloud properties (Stephens, 2005). However, Global Climate Models (GCMs) often assume that clouds are horizontally homogeneous; alternatively, they account for horizontal inhomogeneity using a linear combination of cloudy and clear parts weighted by a cloud fraction, albeit the parameterization of the cloud fraction is highly simplified (Slingo, 1987, 1989; Sundqvist, et al., 1989; Lohmann and Roeckner, 1996; Kiehl et al., 1998). Because realistic and inhomogeneous clouds transport shortwave and longwave radiation quite differently than do the plane-parallel and homogeneous clouds commonly assumed in GCMs, the observed cloud albedo generally is lower than the modeled albedo (Stephens and Greenwald, 1991). As a result, the misrepresentation of inhomegeneous clouds might be a major reason for large uncertainty in estimating anthropogenic aerosol effects on warm clouds (-0.3 to $-1.8\,\mathrm{W\,m^{-2}}$) (IPCC, 2007).

High-resolution atmospheric models, such as, large eddy simulation (LES) models, represent the spatial- and temporal-variations of clouds better than the GCMs. Unfortunately, calculations of radiative transfer in high-resolution models are highly simplified, partly due to the limitation of computer resources. For example, shortwave radiation calculations are often totally ignored (B. Stevens et al., 2001; D. E. Stevens et al., 2002). Therefore, climatically important radiative effects and/or forcings cannot be explored, nor can cloud diurnal cycles be accurately simulated. Moreover, calculations of longwave radiation are reduced to an exponential attenuation of radiative flux with respect to the overlying cloud liquid water path (LWP) with a constant radiative flux at the top of the model domain (e.g., $74\,\mathrm{W\,m^{-2}}$) (B. Stevens et al., 2001; D. E. Stevens et al., 2002). A clear sky radiative cooling is fixed at a rate of $-2\,\mathrm{K\,day^{-1}}$, regardless of atmospheric thermo-dynamic states (Stevens et al., 2002). However, longwave radiative cooling near cloud tops is an important driver for marine stratiform clouds (Stevens et al., 1998, 2001). Clearly, such over-simplified radiation calculations are unrealistic in many aspects.

Furthermore, the complex interactions/feedbacks between clouds, radiation, entrainment, and turbulence are hard to disentangle, and hinder our efforts to better quantify cloud and/or aerosol radiative forcings (IPCC, 2007). For example, the entrainment of

warm, dry air from the free-troposphere could efficiently deplete cloud water, complicate the responses of the cloud LWP to aerosols (Ackerman et al., 2004), and impact aerosol effects on clouds (Guo et al., 2007). However, estimating the entrainment rate of the cloud-topped boundary layer from observational data is challenging and often entails large uncertainties (Caldwell et al., 2005). On the other hand, the entrainment rates estimated from the GEWEX Cloud System Studies (GCSS) models differ by nearly an order of magnitude for only a two-hour simulation of an idealized nighttime marine stratocumulus deck (Moeng et al., 1996). Moreover, compared to various tracer-based estimates made during field campaigns, current parameterizations tend to overestimate entrainment rates (Stevens et al., 2003), as do most Cloud Resolving Models (CRMs) and/or LES models in comparison with the findings from laboratory experiments (Bretherton et al., 1999). Such deficiencies in model studies of the entrainment might be associated with insufficient resolution to capture abrupt changes near inversion layers and to resolve small-scale processes. Numerical representations of clouds, their inhomogeneous structures, and the effects of inhomogeneity on radiative transfer consistently have been poorly assessed due in large part to inadequate resolution in the models.

Many of these deficiencies in GCMs, CRMs, and LESs reflect the limitation on computer resources. In an effort to boost computational sciences, the Brookhaven National Laboratory (BNL) and Stony Brook University lately installed an IBM Blue Gene/L supercomputer at the BNL campus. The Blue Gene/L is a highly scalable multi-node supercomputer, optimized with the scalability and the ability to handle large amounts of data, and so is an extremely efficient tool for large models that can scale to thousands of processors. Accordingly, it can be applied efficiently for computationally expensive atmospheric models with a good scalability, like the Goddard Cloud Ensemble Model (GCE) (Juang et al., 2007). In this study, we took advantage of both the high-performing supercomputer and the scalable GCE to conduct three-dimensional high-resolution simulations to explore how cloud entrainment, cloud-radiation interactions, and cloud radiative-forcing change with model resolution, and to determine the

minimum model resolution necessary to address these issues.

The rest of this paper is organized as follows: Sect. 2 describes the GCE model, the simulation set-up, and the properties of the stratus cloud of interest. Section 3 discusses the numerical simulation results. Section 4 summarizes our results.

2 Model set-up and case description

The three-dimensional parallel version of the Goddard Cloud Ensemble Model (GCE) was selected for this study (Juang et al., 2007). To filter out sound waves, the anelastic approximation was adopted. The current turbulence parameterization (or sub-grid parameterization) was a 1.5-order closure scheme (Tao and Simpson, 1993). The cloud microphysical parameterization was a single-moment bulk scheme that explicitly predicts the mixing ratio of a given water substance (e.g., water vapor, cloud water, and rain water). Cloud droplet effective radius was specified to be 10 μm.

Rather than specifying radiative cooling/heating, online calculations for both shortwave and longwave radiative transfer that are interactively coupled within the atmosphere were used (Tao at al., 2003). The shortwave radiative transfer module used a two-stream Delta-Eddington approximation to calculate the radiative fluxes at the edges of vertical layers. The module has 8 bands covering the ultra-violet- and visible-(UVV) regions from 0.175 μm to 0.700 μm; and 3 absorption bands in the near infra-red (IR) spectrum between 0.700 μm and 10.000 μm. Single O_3 absorption- and Rayleigh-scattering-coefficients are used for each band, so are absorption coefficients (Chou and Suarez, 1999). The surface albedo was fixed at 0.07 in this study, independent of the solar wavelength and/or incidence angles.

The longwave radiative transfer module includes parameterizations for absorptions by H_2O, O_3, and CO_2, and by most minor trace species, e.g., N_2O, CH_4, and CFC's, as well as by warm and ice clouds (Chou et al., 2001). The long-wave spectrum from 0 cm^{-1} to 3000 cm^{-1} is divided into 9 bands and 1 sub-band. Cloud radiative properties are fitted (by regression) to high-spectral resolution extinction coefficients, single

scattering albedos, and asymmetry factors; the properties are then parameterized as functions of cloud water content and droplet effective radius (Chou, et al., 2001). Compared to high spectral-resolution calculations, the atmospheric-heating rates between 0.01 hPa and the surface are accurate to within 5%; the surface radiative fluxes are accurate to within a few $W\,m^{-2}$ (Chou and Suarez, 1999; Chou et al., 2001).

In this study, a stratus cloud sampled on 19 July 2005 during the Marine Stratus/Stratocumulus Experiment (Daum et al., 2008) was simulated. Initially, the boundary layer was well-mixed and capped by a very strong inversion layer (Fig. 1). Temperature decreased linearly from 15.2°C near the surface to 12.2°C at an altitude of 0.39 km, and then increased to 26.1°C at an altitude of 0.60 km. The specific humidity was a constant at about $9.5\,g\,kg^{-1}$ from the ground to 0.39 km, abruptly increased to $12\,g\,kg^{-1}$ up to an altitude of 0.52 km, and then dropped to $1\,g\,kg^{-1}$. This abrupt increase originated in the upward water flux below the inversion. Above the inversion, the free troposphere was warm and dry. The inversion strengths of temperature and moisture were $65°C\,km^{-1}$ and $61\,g\,kg^{-1}\,km^{-1}$, respectively, far stronger than $36°C\,km^{-1}$ and $23\,g\,kg^{-1}\,km^{-1}$ used by Stevens et al. (2001). Clearly, such a strong inversion necessitates high-resolution simulations in order to capture the sharp gradients and the abrupt changes near the inversion layers.

A suite of three-dimensional high-resolution simulations were run. The domain was $6.4\times6.4\,km^2$ horizontally, and 1.25 km vertically. The simulations began at 15:30 LST (local standard time) on 18 July 2005; and the entire simulation period was 32.5 h. We regarded the first 8.5-h as a spin-up time, and mainly performed our analysis over the last 24 h to cover a complete diurnal cycle. We used a time step of 0.5 s or less. The on-line shortwave and longwave radiative transfer modules were called every 1 min, and the model results were archived every 2 min.

Since there are no data on accurate large-scale temperature and moisture forcings for the (model) region of interest (Grabowski et al., 1996), we nudged the domain-average temperature and moisture fields towards their initial states to emulate the impacts of large-scale forcing on the model results; this also balanced the excess radia-

tive and adiabatic cooling/heating as well as surface heat and moisture fluxes. The nudging relaxation timescale is 6 h above the altitude of 0.6 km, and then linearly increases to infinity at the surface (i.e., no nudging forcing), so that the dynamic- and microphysical-evolutions within the boundary layer largely are determined by physical processes (e.g., cloud top radiative cooling, turbulence), rather than by nudging forcing (Guo et al., 2007). The atmosphere was assumed to be cloud free at the beginning of our simulations.

3 Sensitivity tests and model results

Table 1 summarizes 7 sensitivity tests that were performed by changing only the horizontal-grid sizes, changing only the vertical-grid sizes, and simultaneously changing both but with a fixed aspect ratio of horizontal to vertical spacing of 2.5:1. Here, the "X", "Z" and the following number, respectively, denote the horizontal spacing, the vertical spacing, and the spacing size in meters. The time step also varies accordingly to guarantee numerical stability.

3.1 Time series

The intimate interaction between entrainment, clouds, and radiation is an important process within the cloud-topped boundary layer (Yamaguchi and Randall, 2008). However, it is challenging to handle and disentangle it (Ackerman et al., 2004). Moreover, its numerical representations are often dependent on model resolution. In this section, we examine the spatial- and temporal-variations of entrainment, cloud LWP, and cloud top radiative cooling rate. Especially, we explore the dependence of details of this interaction on model resolution.

Since entrainment depends on the efficiency of the mixing between the cloudy air and the above cloud air, and since the inversion layers generally are the interfaces between these two, the variations in the inversion height were examined to approximate

the efficiency of entrainment in this study.

3.1.1 Inversion height (Zi)

The inversion height (Zi) here is defined as the height where the specific humidity is 6.5 g kg^{-1} (Stevens et al., 2002). Figure 2a, b, and c, respectively, presents the time series of domain-average Zi for the sensitivity tests of varying only horizontal grid-spacing (from Δx=25 m to 100 m), varying only vertical grid-spacing (from Δz=10 m to 40 m), and varying both simultaneously (from Δx=25 m and Δz=10 m to Δx=100 m and Δz=40 m). In general, the domain-average Zi exhibits a diurnal cycle, and this diurnal cycle is more significant in more refined resolution runs. The domain-average Zi increases during the night and in the local morning when it can reach up to 0.62 km; it declines in the local afternoon and can fall to 0.60 km. This diurnal cycle conforms to the variations of the entrainment rate based on the analysis of the boundary layer's mass budget of marine stratiform clouds (see Fig. 5 in Caldwell et al., 2005).

The temporal evolutions of the domain-average Zi are very similar when only the horizontal resolution is changed (in the simulations of "X25Z10", "X50Z10", and "X100Z10"). The domain-average Zi tends to increase when Δz increases (Fig. 2b), suggesting that entrainment increases when the vertical resolution decreases (i.e., Δz increases). A higher entrainment at a larger Δz further implies a more effective depletion of cloud water since the air above the cloud layers is very dry and warm with a relative humidity less than 20% (Fig. 1). Changing the horizontal- and vertical-resolution simultaneously with a fixed aspect ratio (Fig. 2c), also causes domain average Zi to increase with decreasing model resolution, and exhibit similar temporal variations as those in the corresponding test with the same Δz (Fig. 2b and c). Hence, our findings suggest that vertical resolution is more important than horizontal resolution in determining entrainment.

Figure 2d, e, and f shows the time series of the standard deviations (σ_{Zi}) associated with the domain averages. With the same Δz=10 m, the temporal variations and magnitudes of σ_{Zi} exhibit very similar comparative characteristics in the tests of "X25Z10",

"X50Z10", and "X100Z10" (Fig. 2d). With the same Δx of 25 m, the magnitudes of σ_{Zi} decrease with increasing Δz (Fig. 2e). In the simulations of changing Δx and Δz proportionally but with a fixed aspect ratio, σ_{Zi} also decreases with increasing Δx (or Δz), and exhibits similar patterns when only Δz increases (Fig. 2e and f). These results reinforce the importance of vertical resolution in modelling entrainment.

Table 2 presents the time-space average Zi and the associated temporal standard deviations in the various resolution runs. When Δz increases, the average Zi increases. This increasing trend of Zi with increasing Δz would help reduce cloud moisture and lower the cloud LWP. When Δx increases, the time-average Zi tends to drop slightly.

The demonstrated higher sensitivity of entrainment to vertical- than to horizontal-resolution led to conduct an additional test, denoted as "X25Z5" with finer vertical resolution (Δz=5 m and Δx=25 m). It turns out that both the magnitude of Zi and its spatial- and temporal-variations in "X25Z5" were very close to those in "X25Z10", suggesting that these two simulations tend to converge. Accordingly, the simulation "X25Z10" is used as a benchmark run in the following discussion.

3.1.2 Liquid water path (LWP)

Entrainment (drying) can reduce the cloud LWP, a cloud property of climatic importance (Stephens, 1978). Figure 3 displays the temporal variations of the domain-average cloud LWP and its standard deviation (σ_{LWP}). All the simulations exhibit qualitatively similar temporal variations in both the domain-average LWP and σ_{LWP} with significant diurnal changes. The cloud LWP reaches its maximum in the local early morning (up to 120 g m^{-2} around 07:00 LST) and its minimum around local noon (~20 g m^{-2} around 12:00 LST). This is consistent with the strengthened instability induced by the cloud top radiative cooling at night, and the cloud dissipation by solar heating as daytime progresses. The results also might suggest that the frequently observed diurnal cycles of cloud properties are largely attributable to shortwave- and longwave-radiative effects. The longwave cooling increases relative humidity and allows more cloud water to form.

Quantitatively, with the same vertical spacing Δz, the domain-average LWP and σ_{LWP} consistently decrease when Δx increases from 25 m to 100 m (Fig. 3a and d). With the same horizontal spacing of Δx and/or the same aspect ratio of Δx to Δz, the domain-average LWP and σ_{LWP} decrease with increasing Δz. The decreasing rate in the LWP is slower when only Δz increases (Fig. 3b) compared to that when both Δz and Δx increase (Fig. 3c), although their temporal trends are very close. Thus, the daily average of the domain-average LWP can reach 74 g m^{-2} in the run of "X25Z10", while it is reduced to only 39 g m^{-2} in the coarsest run of "X100Z40" (Table 2). This almost doubling of the cloud LWP in the simulation with a higher vertical resolution partly reflects a less efficient drying arising from the entrainment-mixing of the dry free-troposphere air (Figs. 1 and 2). As will be discussed later, another possible mechanism involved is a positive feedback between the cloud LWP and radiative cooling. The general decrease of σ_{LWP} with decreasing model resolution suggests that in a lower-resolution simulation, more small-scale processes are unresolved and thus smeared out, so generating a more spatially homogeneous cloud (Fig. 3d, e, and f).

3.1.3 Cloud top radiative cooling

Previous studies showed that the cloud LWP is intimately related to the longwave radiative cooling near cloud top, which, in turn, is an important driver for the cloud-topped marine boundary layer with no/little drizzle and little wind shear (Moeng et al., 1996; Stevens et al., 1998). To examine the sensitivity of the cloud radiative cooling to the model resolution, the time series of the domain-average cloud top radiative cooling rates for tests of "X25Z10" and "X100Z40" has been plotted (Fig. 4). Although their cooling rates are qualitatively similar and both exhibit significant diurnal cycles in both runs, their magnitudes differ substantially. The cooling rate is enhanced by 50% when the vertical spacing Δz is decreased from 40 m to 10 m (Fig. 4a). The reason is that the coarse vertical resolution (e.g., 40 m) smears out some local extremes of the divergence of the radiative flux near the cloud top. We note that the cooling rates in the other sensitivity tests fall generally between "X25Z10" and "X100Z40", and decrease

with decreasing resolution (omitted here for clarity).

Table 2 provides the time averages of the cloud top radiative cooling rates in different sensitivity tests; these rates are comparable in simulations with the same vertical resolution. For example, the cooling rates are 2.42, 2.38, and 2.39 $K\,h^{-1}$, respectively, in "X25Z10", "X50Z10", and "X100Z10", and differ less than 2%. However, the cooling rate becomes smaller for a larger Δz. The average cooling rates are about 2.4, 2.1, and 1.7 $K\,h^{-1}$ for Δz=10 m, 20 m, and 40 m, respectively. It is speculated that stronger cloud top cooling induces stronger downdrafts and updrafts. Accordingly, the magnitudes of vertical motions within the boundary layer generally are larger in higher resolution runs, and can differ by a factor of ~2 (Table 2). Furthermore, the stronger vertical motions can transport water vapor more efficiently from lower troposphere to cloud layers, and enhance cloud moisture and the cloud LWP. The enhanced LWP further enhances radiative cooling, vertical motions, moisture supply, and the LWP itself, suggesting there is a chain of positive feedbacks between radiative cooling and cloud LWP. To quantify the strength of this feedback, we calculated the correlation coefficient between these two as 0.75 (Fig. 4b). It seems to be insensitive to model resolution. On the other hand, the increased radiative cooling could also increase the relative humidity and then could enhance cloud water to form. We also conducted additional sensitivity tests without longwave radiative cooling, and found that the simulated cloud LWP is reduced substantially, and the difference in different resolution runs is negligibly small.

In contrast to this positive feedback, the cloud top radiative cooling also could indirectly, but negatively influence the LWP through entrainment drying. Enhanced cloud top cooling would promote more efficient entrainment drying, and thus reduce the LWP. However, vertical resolution outweighs such an effect. Consequently, with increasing model resolution, reduced entrainment drying in concert with stronger cloud top cooling leads to an even higher LWP (Fig. 3).

3.2 Cloud radiative forcing

One goal of examining the cloud properties and related processes (such as the LWP, entrainment, and the cloud top cooling rate) is to explore their crucial radiative effects on shaping the Earth's climate. Cloud radiative forcing was stressed as one of the key uncertainties in modeling climate (IPCC, 2007), because its understanding is far from complete (especially the contribution from low clouds). To examine the effect of model resolution on this quantity, Fig. 5 illustrates the time series of shortwave- (SW), longwave- (LW), and net- (SW+LW) cloud radiative forcing at the top-of-the-atmosphere (TOA, 0.01 hPa), and at the surface (SRF). Here, the cloud forcing is evaluated as the difference of the downwelling radiative fluxes between the cloudy and the clear atmosphere under the same thermo-dynamic and meteorological backgrounds. The shortwave cloud radiative forcing exposes a significant diurnal variation, the magnitude of which reaches its local maxima around 08:00 LST and 14:00 LST rather than local noon (Figs. 5a and d). This is due to the tradeoff between solar insolation and the cloud LWP which achieves its maximum around 07:00 LST and its minimum around local noon (Fig. 3). The magnitude of the SW forcing at the TOA is smaller than that at the surface, mainly because of the clouds' absorption of the incoming solar radiation. The magnitude of the SW forcing is larger in the higher resolution run of "X25Z10" than those in "X100Z40", principally because the cloud LWP in "X25Z10" is larger.

Compared to SW forcing, the LW cloud radiative-forcing exhibits smaller diurnal variations, especially at the TOA (Fig. 5b and e); at the TOA it is almost $0\,W\,m^{-2}$ because of the small temperature contrast between the low-level cloud top and its underlying surface. The LW forcings are positive, signifying that the cloud traps a portion of the outgoing LW radiative flux. The magnitude of the LW forcing at the surface is smaller in "X100Z40" than that in "X25Z10" (Fig. 5e), and their difference is larger before local noon than afterwards (4.2 vs. $2.5\,W\,m^{-2}$). This difference is ascribed to the difference in the cloud LWP (Fig. 2c).

The net cloud radiative forcings exhibit temporal trends similar to those of the SW

forcings. For daily averages, the net forcings are negative, i.e., cooling is the overall effect of this stratus cloud. The amplitude of the temporal variation of the net forcing is larger by about 15% at the surface than at the TOA (Table 2), due to the stronger negative SW and positive LW forcings at the surface.

Consistent with the simulated cloud LWP, it has been showed that the magnitude of the net cloud radiative forcing increases with increasing model resolution. The daily average net forcings at the TOA are −82 and −121 $W m^{-2}$ in tests of "X100Z40" and "X25Z10", respectively; and the net forcings at the surface are −20 and −60 $W m^{-2}$, respectively. These differ by about 40 $W m^{-2}$, where the differences in the SW and LW forcings are about 40 $W m^{-2}$ and a couple of $W m^{-2}$, respectively. Undoubtedly, the difference in the SW forcing dominates, and the SW forcing is more influenced by the model resolution than the LW forcing. Therefore, the model resolution is expected to be important for estimating radiative forcing where the SW contribution is significant. For example, global average aerosol indirect forcing could change from −1.7 to −2.4 $W m^{-2}$ (with a relative difference of 42%), when the horizontal resolution is coarsened from 2.8° × 2.8° to 4.5° (latitude) × 7.5° (longitude) (Ghan et al., 2001).

3.3 Model resolution and interactions/feedbacks

The preceding analyses suggest that the interactions/feedbacks among the entrainment (inversion height), the cloud LWP, the cloud top radiative cooling, and the cloud radiative forcing are intertwined with one another, and depend on the model resolution in a complex way. Figure 6 schematically depicts the major interactions/feedbacks revealed by this study. With increasing model resolution, the trend of increasing inversion height becomes slower, which implies weaker entrainment drying and helps increase the cloud LWP. More importantly, there exists a positive feedback between the cloud LWP and the cloud top radiative cooling. Increasing model resolution could better resolve local extremes of the cloud top radiative cooling rate. Larger radiative cooling would enhance convection strength and relative humidity and thereby the cloud LWP, which, in turn, would further enhance the cloud top radiative cooling and the LWP it-

self. It is noted that stronger radiative cooling also could enhance entrainment (drying), which is, however, outweighed by the effect of model resolution. Consequently, less entrainment drying and larger radiative cooling with increasing model resolution lead to a larger cloud LWP; the larger LWP results in a stronger cloud radiative forcing both at the TOA and at the surface (Fig. 6).

These results highlight the critical importance of model resolution and positive feedback (chain) in modeling clouds and estimating their radiative forcing. This positive feedback (between clouds and radiative cooling) is able to magnify small differences initiated by the differences in model resolution, and entails substantial discrepancies in the simulated cloud properties and their radiative forcing. These results also offer compelling evidence of the need to use appropriate model resolution, and to couple interactively (rather than specify) shortwave- and longwave-radiative cooling/heating with cloud fields in the model studies of clouds and cloud-related processes.

4 Concluding remarks and discussion

A suite of numerical simulations of a marine stratus cloud were made using the 3-D NASA Goddard GCE model at different model resolution on the IBM Blue Gene supercomputer at the Brookhaven National Laboratory. The main purpose was to explore the sensitivities of entrainment (inversion height), cloud liquid water path (LWP), radiative cooling, and cloud radiative-forcing to model resolution. In this study, an interactive radiative transfer package was fully coupled with the cloud fields and a complete diurnal cycle was examined.

The simulated stratus deck exhibited a significant diurnal cycle, for example, the inversion height, the cloud LWP, and the cloud top radiative cooling rate reached their maxima in the local (early) morning, and their minima around local noon or in the early local afternoon.

The inversion height is more sensitive to vertical- than to horizontal-resolution. When the vertical resolution was coarsened, the time-space average Zi increased and the

diurnal variations in Zi were less significant. When the horizontal resolution was coarsened, the time-space average Zi decreased slightly and the diurnal variations remain very similar. These results suggest that high vertical resolution is critical to resolving entrainment (related) processes, and also suggest that the possible overestimation of the entrainment rate by many models could be alleviated by increasing vertical resolution and/or sacrificing horizontal resolution.

The modelled cloud LWP increases with increasing model resolution. Its time-space average could be doubled when both the horizontal- and vertical-resolution are changed by a factor of 4. This increase was also associated with positive feedback from cloud top radiative cooling. Stronger radiative cooling is conducive to stronger convection and a higher LWP, which, in turn, would strengthen the cooling further. This finding is indicative of an intimate (direct) interplay between clouds and radiative cooling (Fig. 6). Contrary to this positive feedback, a stronger cooling also could reduce the LWP by enhancing entrainment drying. Nevertheless, the entrainment drying seems more dependent on vertical resolution than on the radiative cooling. Less entrainment drying with increasing resolution, together with stronger cooling near cloud top, enhances the LWP. These results stress the profound importance of physically realistic feedback chains, model resolution, and their competing effects on cloud properties. Small differences introduced by different model resolution could be magnified substantially by the positive cloud-radiation feedback chain, and further exacerbated by the effects of model resolution on the entrainment.

With increasing model resolution, the magnitudes of net-, shortwave-, and longwave-cloud radiative forcings increase. The net forcing could differ by 40 $\mathrm{W\,m^{-2}}$ after changing model resolution by a factor of 4. The larger the difference in the LWP, the more the forcing changes. The difference in the net forcing comes mainly from changes in shortwave forcing, because shortwave forcing is more sensitive to model resolution than the longwave forcing. This implies that model resolution is a potential contributor to the large uncertainties in estimating radiative forcing where the shortwave contribution is important; e.g., in aerosol direct and indirect forcings. Although, at first glance,

longwave radiative forcing (per se) is less sensitive to the model resolution, the possibility that climatic responses dependent on the longwave forcing are sensitive to model resolution cannot be ruled out. For example, the climate sensitivity to increased CO_2 concentration could be either enhanced or reduced with increasing horizontal resolution from different GCM simulations (May and Roeckner, 2001; Kiehl et al., 2006).

The varying sensitivities of cloud and/or climate related properties to model horizontal- and vertical-resolution reflect many specific physical processes (e.g., entrainment), positive feedback chains (e.g., clouds and radiation), and nonlinear coupling of multiple processes and effects (e.g., feedbacks and resolution). Depending on scientific questions and concerns, appropriate model resolution should be used, and physical processes should be represented as realistically as possible with affordable computational expenses.

Acknowledgements. This research utilized resources at the New York Center for Computational Sciences at Stony Brook University/Brookhaven National Laboratory which is supported by the US Department of Energy under Contract No. DE-AC02-98CH10886 and by the State of New York.

Guo, Liu, and Daum are supported by the Atmospheric Radiation Measurements (ARM) Program and Atmospheric Sciences Program (ASP) of the US Department of Energy under Contract No. DE-AC02-98CH1-886. Tao, Li, and Zeng are partially supported by the Office of Science (BER), and US Department of Energy/Atmospheric Radiation Measurement (DOE/ARM) Interagency Agreement No. DE-AI02-04ER63755. The GCE model is mainly supported by the NASA Headquarters Atmospheric Dynamics and Thermodynamics Program and the NASA Tropical Rainfall Measuring Mission (TRMM). The authors are grateful to Kiran Alapaty at DOE/ARM, Ashley Williamson at DOE/ASP, and R. Kakar at NASA headquarters for their support of this research.

References

Ackerman, A. S., Kirkpatrick, M. P., Stevens, D. E., and Toon, O. B.: The impact of humidity above stratiform clouds on indirect aerosol climate forcing, Nature, 432, 1014–1017, 2004.

Bretherton, C. S., Macvean, M. K., Bechtold, P., et al.: An intercomparison of radiatively driven entrainment and turbulence in a smoke cloud, as simulated by different numerical models, Q. J. Roy. Meteor. Soc., 125, 391–423, 1999.

Cahalan, R. F., Ridgway, W., Wiscombe, W. J., and Bell, T. L.: The albedo of fractal stratocumulus clouds, J. Atmos. Sci., 51(16), 2434–2455, 1994.

Caldwell, P., Bretherton, C. S., and Wood, R.: Mixed-layer budget analysis of the diurnal cycle of entrainment in Southeast Pacific Stratocumulus, J. Atmos. Sci., 62, 3775–3791, 2005.

Chen, T., Rossow, W. B., and Zhang, Y.: Radiative effects of cloud-type variations, J. Climate, 13, 264–286, 2000.

Chou, M. and Suarez, M.: A solar radiation parameterization for atmospheric studies, Tech. Rep. Series on global modeling and data assimilation, NASA/TM-1999-104606, Vol. 15, Goddard Space Flight Center, 1999.

Chou, M., Suarez, M., Liang, X., and Yan, M.-H.: A thermal infrared radiation parameterization for atmospheric studies, Tech. Rep. Series on global modeling and data assimilation, NASA/TM-2001-104606, Vol. 19, Goddard Space Flight Center, 2001.

Daum, P. H., Liu, Y., McGraw, R. L., Lee, Y., Wang, J., Senum, G., Miller, M., and Hudson, J. G.: Microphysical Properties of Stratus/stratocumulus Clouds During the 2005 Marine Stratus/Stratocumulus Experiment (MASE), J. Geophys. Res., in review, 2008.

Ghan, S. J., Easter, R. C., Chapman, E., Abdul-Razzak, H., Zhang, Y., Leung, L. R., Laulainen, N. S., Saylor, R. D., and Zaveri, R. A.: A physically based estimate of radiative forcing by anthropogenic sulfate aerosol, J. Geophys. Res., 106(D6), 5279–5293, 2001.

Grabowski, W. W., Wu, X., and Moncrieff, M. W.: Cloud resolving modeling of tropical systems during Phase III of GATE. PART I: Two-dimensional experiments, J. Atmos. Sci., 53, 3684–3709, 1996.

Guo, H., Penner, J. E., Herzog, M., and Pawlowska, H.: Examination of the aerosol indirect effect under contrasting environments during the ACE-2 experiment, Atmos. Chem. Phys., 7, 535–548, 2007, http://www.atmos-chem-phys.net/7/535/2007/.

IPCC, Climate Change 2007: The physical science basis, Contribution of Working Group I to the fourth assessment report of the Intergovernmental Panel on Climate Change, Cambridge Univ. Press, Cambridge, United Kingdom and New York, NY, USA, 2007.

Juang, H. M. H., Tao, W.-K., Zeng, X., and Shie, C.-L.: Parallelization of the NASA Goddard Cumulus Ensemble Model for Massively Parallel Computing, Terr. Atmos. Ocean. Sci., 18(3),

593–622, 2007.
Kiehl, J. T., Hack, J. J., Bonan, G. B., Boville, B. B., Williamson, D. L., and Rasch, P. J.: The National Center for Atmospheric Research Community Climate Model: CCM3, J. Climate, 11, 1131–1149, 1998.
Kiehl, J. T., Shields, C. A., Hack, J. J., and Collins, W. D.: The climate sensitivity of the Community Climate System Model version 3 (CCSM3), J. Climate, 19(11), 2584–2596, 2006.
May, W. and Roeckner, E.: A time-slice experiment with the ECHAM4 AGCM at high resolution: The impact of horizontal resolution on annual mean climate change, Clim. Dynam., 17(5–6), 407–420, 2001.
Lohmann, U. and Roeckner, E.: Design and performance of a new cloud microphysics scheme developed for the ECHAM general circulation model, Clim. Dynam., 12, 557–572, 1996.
Moeng, C.-H., Cotton, W. R., Bretherton, C., Chlond, A., Khairoutdinov, M., Krueger, S., Lewellen, W. S., MacVean, M. K., Pawquier, J. R. M., Rand, H. A., Siebesma, A. P., Stevens, B., and Sykes, R. I.: Simulation of a stratocumulus-topped planetary boundary layer Intercomparison among different numerical codes, B. Am. Meteorol. Soc., 77, 261–278, 1996.
Slingo, J. M.: The development and verification of a cloud prediction scheme for the ECMWF model, Q. J. Roy. Meteor. Soc., 113, 899–927, 1987.
Slingo, A.: A GCM parameterization for the shortwave radiative properties of water clouds, J. Atmos. Sci., 46, 1419–1427, 1989.
Stephens, G. L.: Radiative profiles in extended water clouds. II: parameterization schemes, J. Atmos. Sci., 35(11), 2123–2132, 1978.
Stephens, G. L. and Greenwald, T. J.: The earth's radiation budget and its relation to atmospheric hydrology observations of cloud effects, J. Geophys. Res., 96(D8), 15 325–15 340, 1991.
Stephens, G. L.: Cloud feedbacks in the climate system: A critical review, J. Climate, 18, 237–273, 2005.
Stevens, B., Cotton, W. R., Feingold, G., and Moeng, C.-H.: Large-eddy simulations of strongly precipitating, shallow, stratocumulus-toped boundary layers, J. Atmos. Sci., 55, 3616–3638, 1998.
Stevens, B., Ackerman, A. S., Albrecht, B. A., Brown, A. R., Chlond, A., Cuxart, J., Duynkerke, P. J., Lewellen, D. C., Macvean, M. K., Neggers, R. A. J., Sànchez, E., Siebesma, A. P., and Stevens, D. E.: Simulations of trade wind cumuli under a strong inversion, J. Atmos. Sci., 58, 1870–1891, 2001.

Stevens, B., Lenschow, D. H., Vali, G., Gerber, H., et al.: Dynamics and chemistry of marine stratocumulus-DYCOMS-II, B. Am. Meteorol. Soc., 84, 579–593, 2003.

Stevens, D. E., Ackerman, A. S., and Bretherton, C. S.: Effects of domain size and numerical resolution on the simulation of shallow cumulus convections, J. Atmos. Sci., 59, 3285–3301, 2002.

Sundqvist, H., Berge, E., and Kristjansson, J. E.: Condensation and cloud parametrization studies with a mesoscale numerical weather prediction model, Mon. Weather Rev., 117, 1641–1657, 1989.

Tao, W.-K. and Simpson, J.: Goddard Cumulus Ensemble Model, Part I: Model description, Terr. Atmos. Ocean. Sci., 4(1), 35–72, 1993.

Tao, W.-K., Simpson, J., Baker, D., Braun, S., Chou, M.-D., Ferrier, B., Johnson, D., Lang, S., Khain, A., Lynn, B., Shie, C.-L., Starr, D., Sui, C.-H., Wang, Y., and Wetzel, P.: Microphysics, radiation, and surface processes in the Goddard Cumulus Ensemble (GCE) model, A Special Issue on Non-hydrostatic Mesoscale Modeling, Meteorol. Atmos. Phys., 82, 97–137, 2003.

Yamaguchi, T. and Randall, D. A.: Large-eddy simulation of evaporatively driven entrainment in cloud-topped mixed layers, J. Atmos. Sci., 65, 1481–1504, 2008.

Table 1. Summary of simulations with different horizontal and vertical spacings.

simulations	Δx=Δy (m)	Δz (m)
"X25Z10"	25	10
"X50Z10"	50	10
"X100Z10"	100	10
"X25Z20"	25	20
"X25Z40"	25	40
"X50Z20"	50	20
"X100Z40"	100	40

Table 2. Time-space averages of the inversion height (Zi), the cloud liquid water path (LWP), the cloud top radiative cooling rate, the magnitude of the vertical velocity (W) within the boundary layer (from surface to an altitude of 0.40 km), the net (SW+LW) cloud radiative forcing at the top-of-the-atmosphere (TOA, 0.01 hPa) , and the net cloud radiative forcing at the surface; the associated standard deviations are indicated in parenthesis for the sensitivity tests with different horizontal- and vertical-resolution.

	Zi (m)	LWP ($g\,m^{-2}$)	cooling rate ($K\,h^{-1}$)	W ($m\,s^{-1}$)	TOA forcing ($W\,m^{-2}$)	SRF forcing ($W\,m^{-2}$)
"X25Z10"	606	73.9	2.42	0.26	−121	−60
	(6)	(30)	(0.45)	(0.08)	(123)	(140)
"X50Z10"	604	62.8	2.38	0.24	−108	−46
	(5)	(26)	(0.42)	(0.07)	(113)	(128)
"X100Z10"	603	53.9	2.39	0.21	−102	−40
	(5)	(22)	(0.35)	(0.06)	(108)	(122)
"X25Z20"	608	60.5	2.13	0.23	−110	−47
	(6)	(22)	(0.37)	(0.07)	(109)	(125)
"X25Z40"	609	44.0	1.70	0.17	−92	−30
	(5)	(14)	(0.30)	(0.06)	(90)	(104)
"X50Z20"	607	55.2	2.12	0.21	−101	−38
	(5)	(21)	(0.38)	(0.07)	(103)	(117)
"X100Z40"	609	39.1	1.67	0.14	−82	−20
	(5)	(14)	(0.30)	(0.07)	(81)	(93)

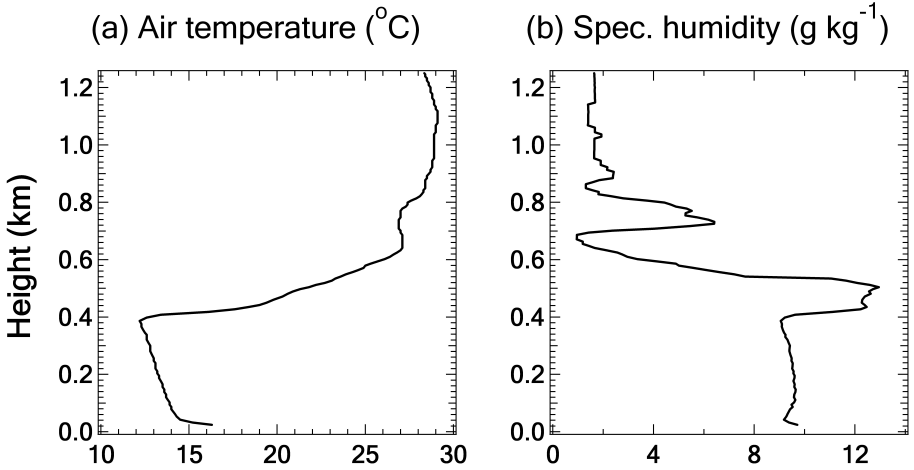

Fig. 1. The initial profiles from the radiosonde sounding around 15:30 LST on 18 July 2005; **(a)** the air temperature, and **(b)** the specific humidity.

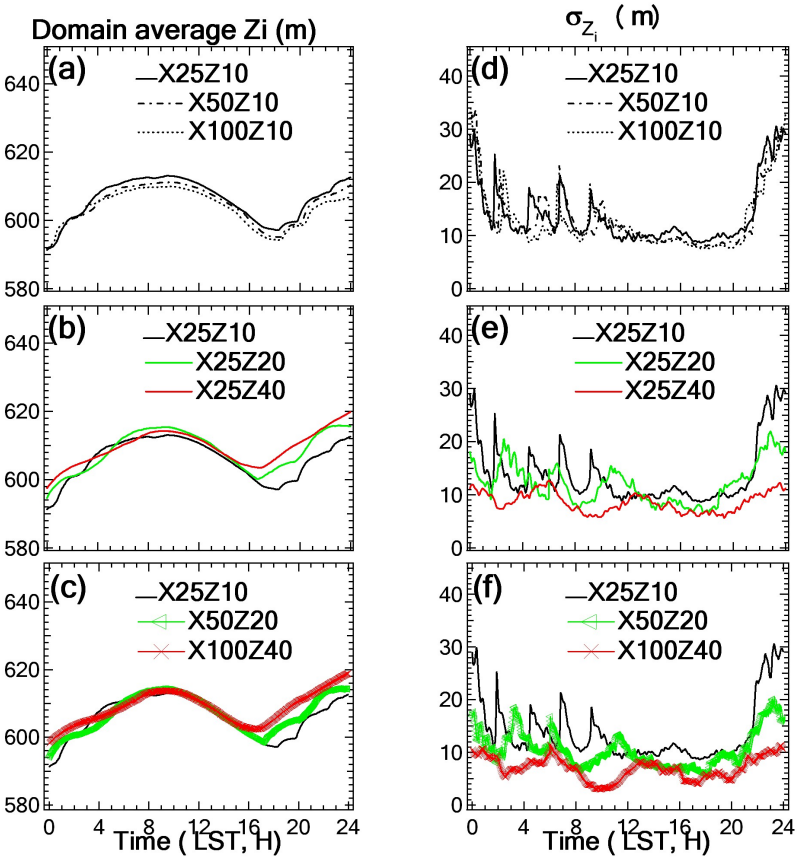

Fig. 2. Time series of the domain-average inversion height (Zi, **a, b, c**) and its associated standard deviation (σ_{Zi}, **d, e, f**) for the sensitivity tests of varying horizontal resolution (a, d), of varying vertical resolution (b, e), and of varying horizontal- and vertical-resolution simultaneously but with a fixed aspect ratio of horizontal-to-vertical spacing of 2.5 (c, f).

ACPD
8, 20399–20425, 2008

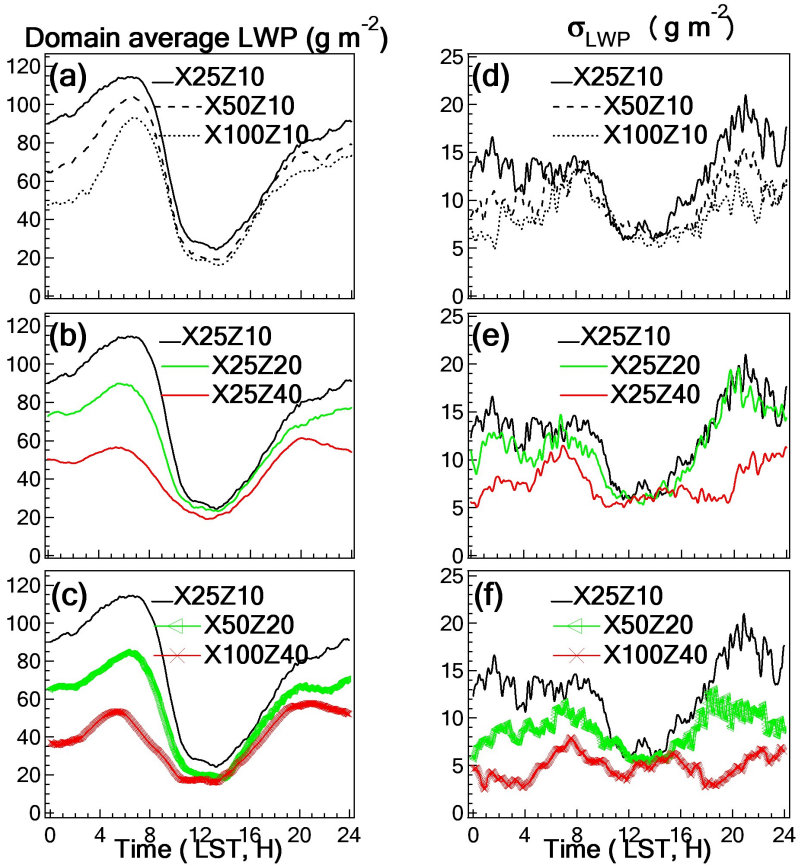

Fig. 3. The same as in Fig. 2, but for the cloud liquid water path (LWP).

ACPD
8, 20399–20425, 2008

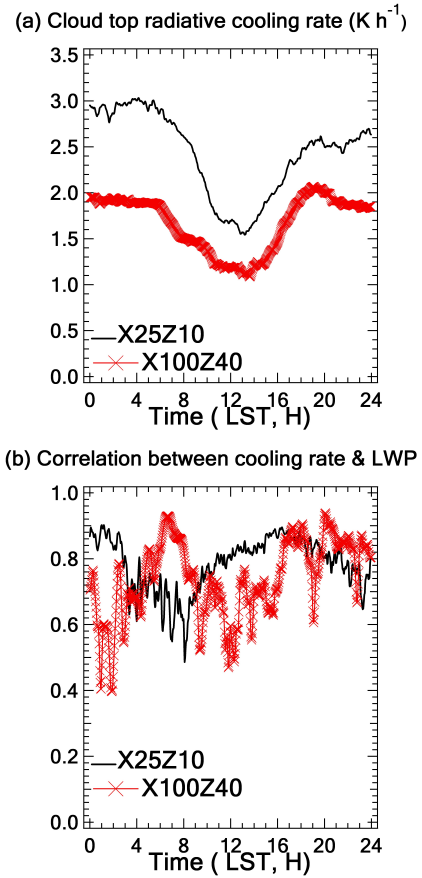

Fig. 4. Time series of the domain averages of the cloud top radiative cooling rate in **(a)**, and the correlation between the cloud top radiative cooling rate and the cloud liquid water path (LWP) in **(b)** in tests of "X25Z10" (black) and "X100Z40" (red).

ACPD
8, 20399–20425, 2008

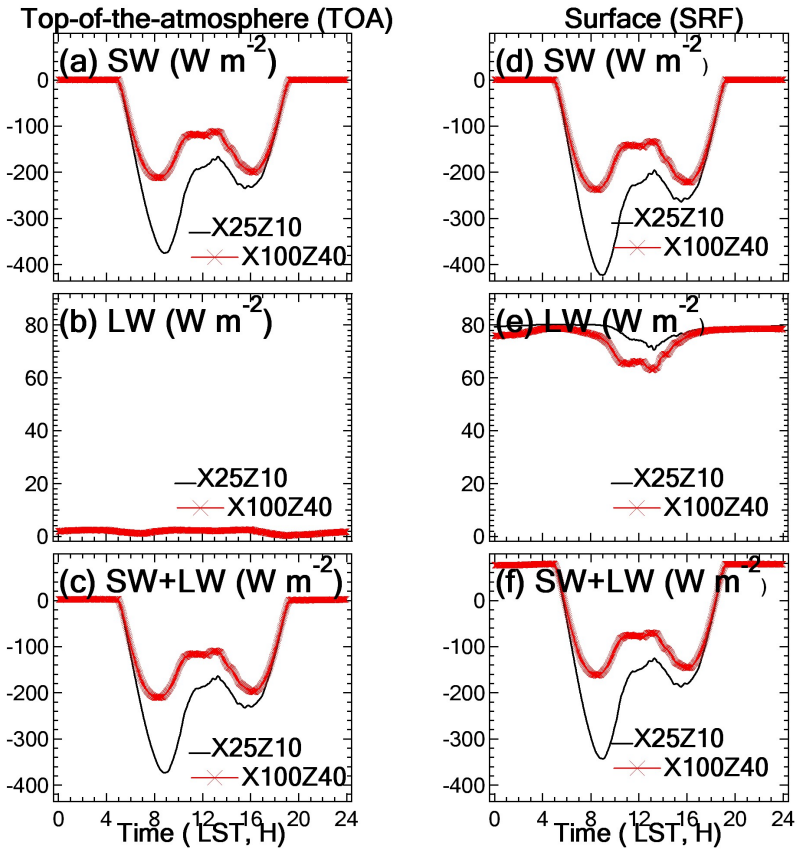

Fig. 5. Time series of the shortwave (SW), the longwave (LW), and the net (SW+LW) cloud radiative forcings at the top-of-the-atmosphere (TOA, **a, b, c**) and at the surface (SRF, **d, e, f**) in tests of "X25Z10" (black) and "X100Z40" (red). (Note: The LW forcings at the TOA in tests of "X25Z10" and "X100Z40" are so similar that two curves almost overlap in b.)

ACPD
8, 20399–20425, 2008

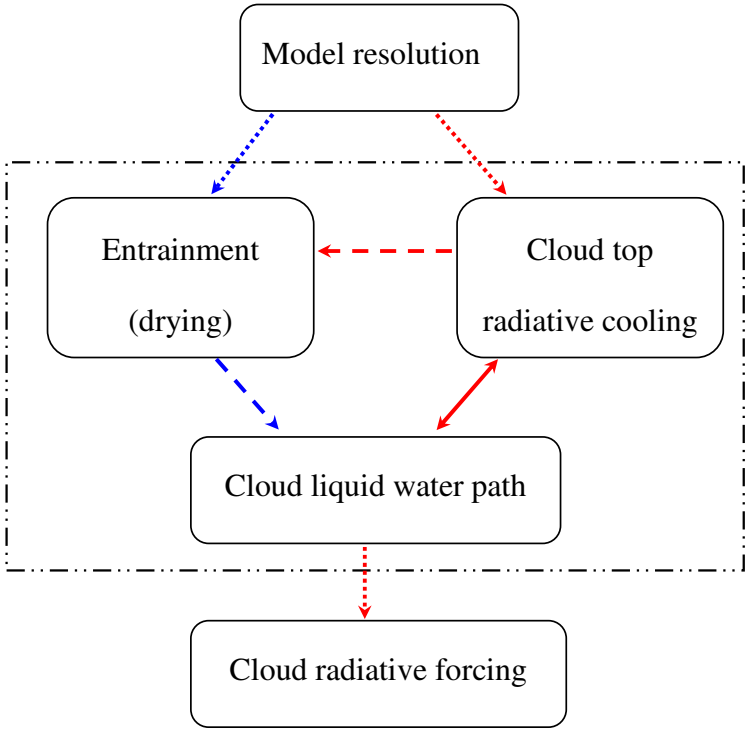

Fig. 6. Schematic diagram showing the interaction between entrainment, cloud top radiative cooling, and cloud liquid water path (in a rectangular box); and the effects of model resolution on this interaction and on the cloud radiative forcing. A single arrow with a dash line indicates a one-way interaction, and double arrows with a solid line indicate a two-way interaction; Red means a positive interaction and blue means a negative one; A red arrow with a dotted line means a positive effect; A blue arrow with a dotted line means a negative one.

ACPD
8, 20399–20425, 2008